




# Flat bands and magnetism in $\text{Fe}_4\text{GeTe}_2$ and $\text{Fe}_5\text{GeTe}_2$ due to bipartite crystal lattices

Fuyi Wang  and Haijun Zhang 

National Laboratory of Solid State Microstructures, School of Physics, Nanjing University, Nanjing 210093, China  
and Collaborative Innovation Center of Advanced Microstructures, Nanjing University, Nanjing 210093, China

 (Received 11 July 2023; revised 7 October 2023; accepted 6 November 2023; published 20 November 2023)

$\text{Fe}_{n=4,5}\text{GeTe}_2$  exhibits quasi-two-dimensional properties as a promising candidate for a near-room-temperature ferromagnet, which has attracted great interest. In this work, we notice that the crystal lattice of  $\text{Fe}_{n=4,5}\text{GeTe}_2$  can be approximately regarded as being stacked by three bipartite crystal lattices. By combining the model Hamiltonians of bipartite crystal lattices and first-principles calculations, we investigate the electronic structure and the magnetism of  $\text{Fe}_{n=4,5}\text{GeTe}_2$ . We conclude that flat bands near the Fermi level originate from the bipartite crystal lattices and that these flat bands are expected to lead to the itinerant ferromagnetism in  $\text{Fe}_{n=4,5}\text{GeTe}_2$ . Interestingly, we also find that the magnetic moment of the Fe5 atom in  $\text{Fe}_5\text{GeTe}_2$  is distinct from the other Fe atoms and is sensitive to the Coulomb interaction  $U$  and external pressure. These findings may be helpful to understand the exotic magnetic behavior of  $\text{Fe}_{n=4,5}\text{GeTe}_2$ .

DOI: [10.1103/PhysRevB.108.195140](https://doi.org/10.1103/PhysRevB.108.195140)

## I. INTRODUCTION

In recent years,  $\text{Fe}_{n=3,4,5}\text{GeTe}_2$  have been discovered as van der Waals (vdW) itinerant ferromagnets with a high Curie temperature  $T_c$  [1–10]. They are promising for spintronic applications due to the near-room-temperature ferromagnetism, magnetic anisotropy, and high electric conductivity [3–21].  $\text{Fe}_3\text{GeTe}_2$  was first discovered in  $\text{Fe}_{n=3,4,5}\text{GeTe}_2$  family [22,23], and its magnetism and electronic structure have been extensively investigated [24–26].  $\text{Fe}_4\text{GeTe}_2$  and  $\text{Fe}_5\text{GeTe}_2$ , with the space groups of  $R\bar{3}m$  and  $R3m$ , share a similar lattice structure which is distinct from that of  $\text{Fe}_3\text{GeTe}_2$ , and especially  $\text{Fe}_5\text{GeTe}_2$  can be considered to be obtained from inserting one Fe layer into  $\text{Fe}_4\text{GeTe}_2$ . Therefore we mainly focus on  $\text{Fe}_{n=4,5}\text{GeTe}_2$  in this work.  $\text{Fe}_{n=4,5}\text{GeTe}_2$  also exhibit many interesting properties, such as the Kondo effect [27], anomalous Hall effect (AHE) [28,29], butterfly-shaped magnetoresistance [30], controllable topological magnetic transformations [31], and skyrmionic spin structures up to the room temperature [32,33]. However, the underlying physics of the magnetic behaviors of  $\text{Fe}_{n=4,5}\text{GeTe}_2$  has not been well understood.

To investigate the electronic structure and the magnetism of  $\text{Fe}_{n=4,5}\text{GeTe}_2$ , we approximately decompose their crystal lattices into three basic layers due to the layered structure. Each basic layer contains at least one Fe layer and one Ge or Te layer, as shown in Fig. 1. Interestingly, we notice that these basic layers of  $\text{Fe}_{n=4,5}\text{GeTe}_2$  can be approximately regarded as bipartite crystal lattices (BCLs) which can be divided into two sublattices with negligible intrasublattice hopping [34,35], since the hopping primarily occurs between the Fe and Ge/Te sublattices. We determine that the stacked BCLs in  $\text{Fe}_{n=4,5}\text{GeTe}_2$  give rise to flat bands [36–39] which may account for the ferromagnetism observed in these materials. It is worth mentioning that the decomposition of BCLs for  $\text{Fe}_{n=4,5}\text{GeTe}_2$  is a rough approximation, and the hoppings between adjacent BCLs still require careful consideration.

In this work, we construct model Hamiltonians for the stacked BCLs of  $\text{Fe}_{n=4,5}\text{GeTe}_2$ . We determine that the flat bands can be attributed to the BCLs, based on these model Hamiltonians. We also demonstrate that the itinerant ferromagnetism in these materials arises from the nearly flat bands near the Fermi energy driven by the Coulomb interaction  $U$ , which is known as flat-band ferromagnetism [40–46]. The BCL-induced ferromagnetism primarily depends on the lattice structure, orbitals, and electron filling number. We expect that this conclusion could be extended to other vdW ferromagnets. Furthermore, by combining the model Hamiltonians and first-principles calculations, we find that the magnetic moment of Fe5 in  $\text{Fe}_5\text{GeTe}_2$  is sensitive to both  $U$  and external pressures. The pressure-tunable magnetic moment transitions in  $\text{Fe}_5\text{GeTe}_2$  might be experimentally observed.

## II. METHODS

First-principles calculations are carried out using the Perdew-Burke-Ernzerhof-type (PBE) generalized gradient approximation (GGA) [47] of the density functional theory (DFT), using the Vienna *ab initio* simulation package (VASP) [48–50]. We take the GGA +  $U$  method with  $U = 3.0$  eV to investigate the correlation effects. We calculated the total energy for different magnetic states and determined the ferromagnetic ground state of  $\text{Fe}_{n=4,5}\text{GeTe}_2$ . A kinetic energy cutoff of 500 eV is used, and the  $10 \times 10 \times 10$   $k$ -point mesh is taken for the bulk calculations. The experimental lattice constants of  $\text{Fe}_4\text{GeTe}_2$  ( $a = 4.03$  Å, and  $c = 29.08$  Å) [4] and  $\text{Fe}_5\text{GeTe}_2$  ( $a = 4.04$  Å, and  $c = 29.19$  Å) [5] are adopted. The inner atomic positions are obtained via full relaxation with a total energy tolerance of  $10^{-6}$  eV. The Wannier-based model Hamiltonians are obtained from the projection of the  $p$  orbitals of Ge and Te and the  $d$  orbitals of Fe through employing the WANNIER90 package [51–53].

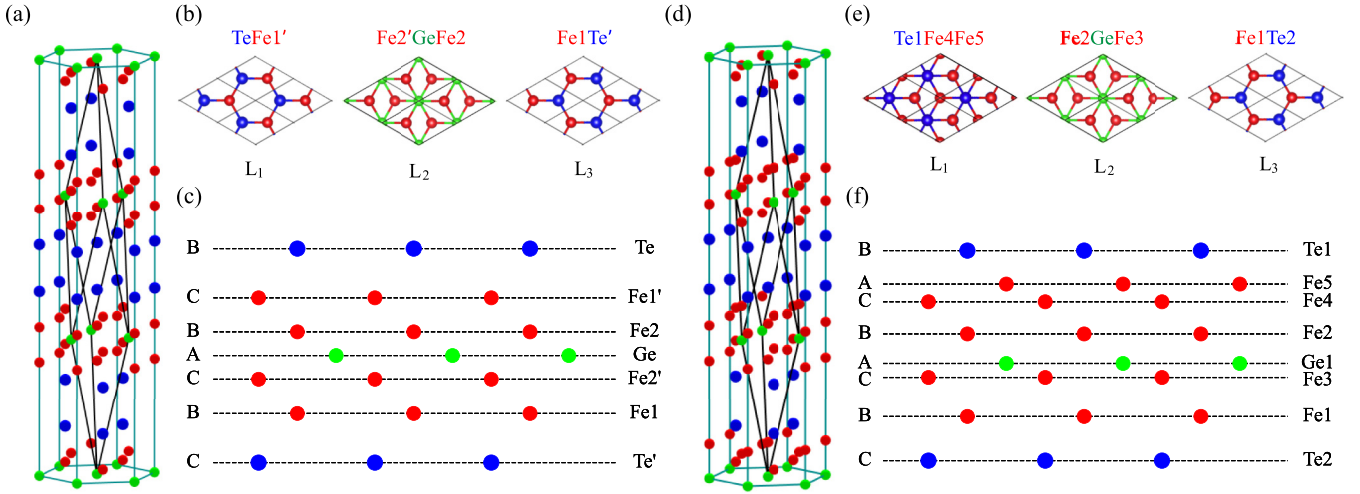


FIG. 1. Crystal structure and bipartite crystal lattices. (a) Crystal structures of  $\text{Fe}_4\text{GeTe}_2$  with primitive lattice cell in black solid line. (b) Top views of three BCLs of  $\text{Fe}_4\text{GeTe}_2$ , labeled  $L_1$ ,  $L_2$  and  $L_3$ . The first BCL ( $L_1$ ) is a honeycomb lattice. The center BCL ( $L_2$ ) is a dice lattice. The third BCL ( $L_3$ ) is equivalent to the  $L_1$  due to the inversion symmetry. (c) The side view of the septuple layer of  $\text{Fe}_4\text{GeTe}_2$ . The triangle lattice has three different stacked positions denoted as  $A$ ,  $B$  and  $C$ . (d) Crystal structures of  $\text{Fe}_5\text{GeTe}_2$  with primitive lattice cell in black solid line. (e) Top view of three BCLs of  $\text{Fe}_5\text{GeTe}_2$ . The first BCL ( $L_1$ ) and the center BCL ( $L_2$ ) are dice lattices. The third BCL ( $L_3$ ) is a honeycomb lattice. (f) The side view of the octuple layer of  $\text{Fe}_5\text{GeTe}_2$ .

### III. CRYSTAL STRUCTURE AND ORBITALS

#### A. The bipartite crystal lattice

$\text{Fe}_4\text{GeTe}_2$  has a space group of  $R\bar{3}m(166)$  that includes an inversion symmetry. The Te ( $\text{Fe1}'$ ,  $\text{Fe2}$ ) atoms are related to the  $\text{Te}'$  ( $\text{Fe1}$ ,  $\text{Fe2}'$ ) atoms via an inversion operation, with the Ge atom serving as the inversion center. The lattice of  $\text{Fe}_4\text{GeTe}_2$  has a septuple-layer structure, as shown in Fig. 1. When we use ABC to represent different stacking positions, the stacking manner of  $\text{Fe}_4\text{GeTe}_2$  in the septuple-layer structure can be expressed as  $\text{Te}(B)\text{-Fe1}'(C)\text{-Fe2}(B)\text{-Ge}(A)\text{-Fe2}(C)\text{-Fe1}'(B)\text{-Te}'(C)$ , as shown in Fig. 1(c). We can decompose the unit cell of  $\text{Fe}_4\text{GeTe}_2$  into three BCLs stacked along the  $z$  direction, denoted as  $L_1$ ,  $L_2$ , and  $L_3$ . The  $L_1$  BCL comprises the  $\text{Fe1}$  sublattice and the  $\text{Te}$  sublattice, while the  $L_3$  BCL comprises the  $\text{Fe1}'$  sublattice and the  $\text{Te}'$  sublattice. The  $L_1$  and  $L_3$  BCLs are related through the inversion symmetry. The  $L_2$  BCL consists of the  $\text{Fe2}(\text{Fe2}')$  sublattice and the  $\text{Ge}$  sublattice, which can be viewed as a dice lattice [34,54–56] with an inversion symmetry, where the  $\text{Ge}$  atom acts as the inversion center.

$\text{Fe}_5\text{GeTe}_2$  belongs to the  $R3m(160)$  space group. The lattice of  $\text{Fe}_5\text{GeTe}_2$  can be obtained by inserting a  $\text{Fe5}$  layer between the  $\text{Fe1}'$  and  $\text{Te1}$  layers of  $\text{Fe}_4\text{GeTe}_2$  [4], as depicted in Figs. 1(c) and 1(f). The inserted  $\text{Fe5}$  layer breaks the inversion symmetry, resulting in the unequivalence of  $\text{Fe1}$  and  $\text{Fe1}'$ , as well as  $\text{Fe2}$  and  $\text{Fe2}'$ . Consequently,  $\text{Fe1}'$  and  $\text{Fe2}'$  in  $\text{Fe}_5\text{GeTe}_2$  are renamed as  $\text{Fe4}$  and  $\text{Fe3}$ , respectively. The lattice of  $\text{Fe}_5\text{GeTe}_2$  has an octuple-layer structure, which can also be approximately decomposed into three BCLs stacked along the  $z$  direction. The stacking manner of  $\text{Fe}_5\text{GeTe}_2$  in the octuple-layer structure can be expressed as  $\text{Te1}(B)\text{-Fe5}(A)\text{-Fe4}(C)\text{-Fe2}(B)\text{-Ge}(A)\text{-Fe3}(C)\text{-Fe1}(B)\text{-Te2}(C)$ , as shown in Fig. 1(f). The  $L_1$  BCL in  $\text{Fe}_5\text{GeTe}_2$  is a dice lattice consisting of the  $\text{Fe4}$  and  $\text{Fe5}$  sublattice and the  $\text{Te1}$  sublattice, though it is just a quasi-BCL due to the non-negligible nearest hopping

between  $\text{Fe4}$  and  $\text{Fe5}$ . The  $L_2$  BCL in  $\text{Fe}_5\text{GeTe}_2$  is a dice lattice but lacks the inversion symmetry. Lastly, the  $L_3$  BCL in  $\text{Fe}_5\text{GeTe}_2$  is a honeycomb lattice which is almost identical to the  $L_3$  BCL in  $\text{Fe}_4\text{GeTe}_2$ .

#### B. Orbitals and the site symmetry

The ferromagnetism in  $\text{Fe}_{n=4,5}\text{GeTe}_2$  is mainly due to the partially filled  $d$  orbitals of  $\text{Fe}$ , whereas  $\text{Te}$  and  $\text{Ge}$  do not exhibit major magnetic behavior. Therefore it is important to analyze the splitting of  $\text{Fe}$ 's  $d$  orbitals to reveal the underlying mechanism of the ferromagnetism.

Both  $\text{Fe}_4\text{GeTe}_2$  and  $\text{Fe}_5\text{GeTe}_2$  have the  $C_{3v}$  site symmetry, which has three irreparable representations: two 1D irreps  $A_{1,2}$  and a 2D irrep  $E$  (Table I). The  $p$  and  $d$  orbitals can be classified based on the irreducible representations (irrep) of the site symmetry group. Here,  $p_z$  corresponds to  $A_1$  irrep for  $p$  orbitals of  $\text{Te}$  and  $\text{Ge}$ , while  $(p_x, p_y)$  corresponds to  $E$  irrep and forms a doublet. Moreover, the  $d$  orbitals of  $\text{Fe}$  are divided into a singlet  $d_{z^2}$  with  $A_1$  irrep and two doublets  $(d_{xz}, d_{yz})$  and  $(d_{xy}, d_{x^2-y^2})$  with  $E$  irrep. The orbitals in doublets can be recombined as  $p_x \pm ip_y$ ,  $d_{xz} \pm id_{yz}$ , and  $d_{x^2-y^2} \pm id_{xy}$ , renamed according to their quantum numbers of the angular momentum projection operator  $\hat{l}_z$  as  $p_{m=\pm 1}$ ,  $d_{m=\pm 1}$ , and  $d_{m=\pm 2}$ . Meanwhile, the singlet orbitals are renamed as  $p_{m=0}$  and  $d_{m=0}$ , respectively.

TABLE I. The character table of the point group  $C_{3v}$ .

	$E$	$C_3(z)$	$3\sigma_z$	$p$ orbitals	$d$ orbitals
$A_1$	1	1	1	$p_z$	$d_{z^2}$
$A_2$	1	1	-1	/	/
$E$	2	-1	0	$(p_x, p_y)$	$(d_{xy}, d_{x^2-y^2}); (d_{xz}, d_{yz})$

Due to the stacking of BCLs along the  $z$  direction, the most significant interactions between adjacent layers are  $\sigma$  bondings formed between the  $p_z$  and  $d_{z^2}$  orbitals, both of which have the quantum numbers  $m = 0$ .

#### IV. MODEL HAMILTONIANS

##### A. Construction of model Hamiltonians

To understand the origin of flat bands, it is essential to formulate a model Hamiltonian. Since the lattice structure of Fe <sub>$n=4,5$</sub> GeTe<sub>2</sub> can be viewed as three stacked BCLs, we construct the tight-binding model Hamiltonian  $H_{\text{tot}}$  by placing the BCL Hamiltonians  $H_{L_i}$  on the diagonal. The general form of the tight-binding model Hamiltonian for Fe <sub>$n=4,5$</sub> GeTe<sub>2</sub> is written as,

$$H_{\text{tot}}(k) = \begin{pmatrix} H_{L_1}(k) & S_{12}(k) & S_{13}(k) \\ S_{12}^\dagger(k) & H_{L_2}(k) & S_{23}(k) \\ S_{13}^\dagger(k) & S_{23}^\dagger(k) & H_{L_3}(k) \end{pmatrix} \quad (1)$$

where the  $S_{12}$  and  $S_{23}$  represent the hopping between adjacent BCLs which usually have the same order of magnitude as the intra-BCL hoppings, while the  $S_{13}$  between the  $L_1$  and  $L_3$  BCLs is almost zero. Therefore the Hamiltonians of  $L_1$ ,  $L_2$ , and  $L_3$  BCLs cannot be treated independently. However, the hopping between adjacent BCLs primarily occurs between orbitals along the  $z$  direction, such as the  $p_z$  and  $d_{z^2}$  with  $m = 0$ . Therefore, to simplify the model, the orbitals can be categorized into two sets. The first set comprises all the orbitals with  $m = 0$ , while the second set consists of the remaining orbitals with  $m \neq 0$ . By applying a unitary transformation, the original model Hamiltonian is transformed to,

$$H_{\text{tot}}(k) = \begin{pmatrix} H_{m=0}(k) & S_m(k) \\ S_m^\dagger(k) & H_{m \neq 0}(k) \end{pmatrix}, \quad (2)$$

where the  $H_{m=0}(k)$  and  $H_{m \neq 0}(k)$  are the Hamiltonian with the  $m = 0$  orbitals and  $m \neq 0$  orbitals, respectively.  $S_m(k)$  is the hopping matrix between the  $m = 0$  and  $m \neq 0$  orbitals. Figures 2(b) and 3(b) show that the band structures calculated by  $H_{m \neq 0}(k)$  of Fe <sub>$n=4,5$</sub> GeTe<sub>2</sub> can catch the main feature of the band structures from the first-principles calculations, which validate the partitioning of orbitals into  $m = 0$  and  $m \neq 0$ . Since the strongest interlayer coupling occurs among the orbitals with  $m = 0$ , we treat  $H_{m=0}(k)$  as a whole without decomposition.

Since the hopping between adjacent BCLs is relatively weak for the  $m \neq 0$  orbitals, the  $H_{m \neq 0}(k)$  is given by

$$H_{m \neq 0}(k) = \begin{pmatrix} H_{B_1}^{m \neq 0}(k) & S_{B_{12}}(k) & 0 \\ S_{B_{12}}^\dagger(k) & H_{B_2}^{m \neq 0}(k) & S_{B_{23}}(k) \\ 0 & S_{B_{23}}^\dagger(k) & H_{B_3}^{m \neq 0}(k) \end{pmatrix}, \quad (3)$$

where  $H_{B_i}^{m \neq 0}$  is the Hamiltonian based on the  $m \neq 0$  orbitals of the  $L_i$  BCL, and  $S_{B_{ij}}$  is the hopping between the  $L_i$  BCL and the  $L_j$  BCL, which can be negligible ( $S_{B_{ij}} \approx 0$ ). Then,  $H_{m \neq 0}(k)$  is further considered to be made up of the three individ-

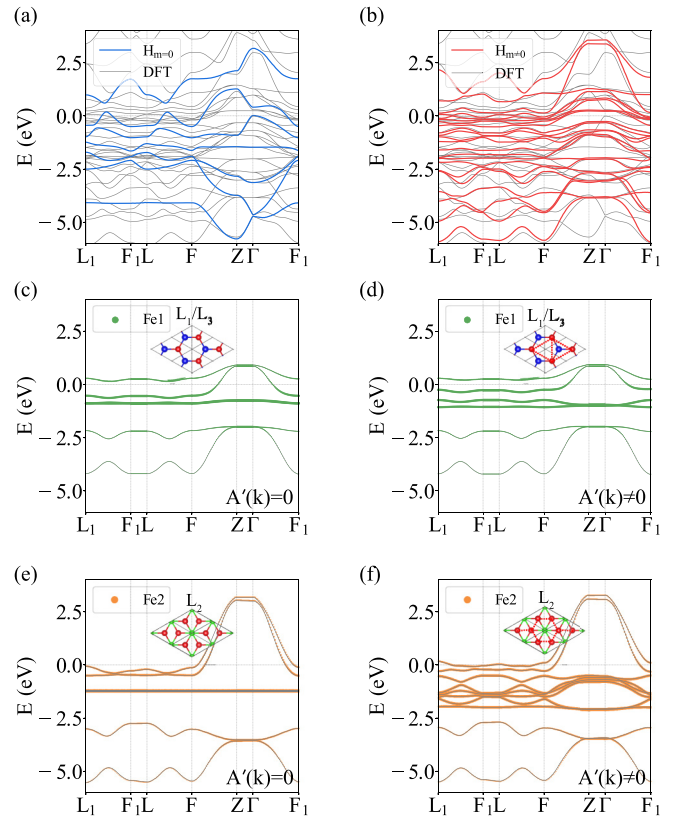


FIG. 2. Band structures by model Hamiltonians of Fe<sub>4</sub>GeTe<sub>2</sub>. [(a) and (b)] The band structures of  $H_{m=0}$  and  $H_{m \neq 0}$  in red and blue. The dashed gray lines are the band structures calculated by first-principles calculations (density functional theory, DFT). [(c) and (d)] Band structures by the  $H_{B_1}/H_{B_3}$  for  $A'(k) = 0$  (c) and  $A'(k) \neq 0$  (d).  $H_{B_1}$  is equivalent to  $H_{B_3}$  due to the inversion symmetry. The projections of Fe1 are in green. [(e) and (f)] Band structures by the  $H_{B_2}$  for  $A'(k) = 0$  (e) and  $A'(k) \neq 0$  (f). The projections of Fe1 are in orange.

ual  $H_{B_i}^{m \neq 0}$  which is written as [35],

$$H_{B_i}^{m \neq 0}(k) = \begin{pmatrix} A(k) & S(k) \\ S^\dagger(k) & B(k) \end{pmatrix}, \quad (4)$$

where  $A(k)/B(k)$  is a Hermitian matrix denoting the onsite energy and intrasublattice hopping and  $S(k)$  denotes the inter-sublattice hopping for each BCL. Since onsite energies lie on the diagonal, the matrix  $A'(k)/B'(k)$  obtained after removing the diagonal terms of  $A(k)/B(k)$  represents the intrasublattice hoppings. As mentioned above, the decomposition of BCLs of Fe <sub>$n=4,5$</sub> GeTe<sub>2</sub> is a rough approximation due to the existence of the nonzero intrasublattice hoppings which leads to the dispersion of flat bands.

##### B. Flat bands due to BCLs

In general, a BCL Hamiltonian can induce ( $N = N_A - N_B$ ) flat bands when  $N_A > N_B$  [35], as shown in Appendix A. Here,  $N_{A/B}$  denotes the number of orbitals present on the  $A/B$  sublattice. The emergence of flat bands can be attributed to the destructive interference of wavefunctions associated with the



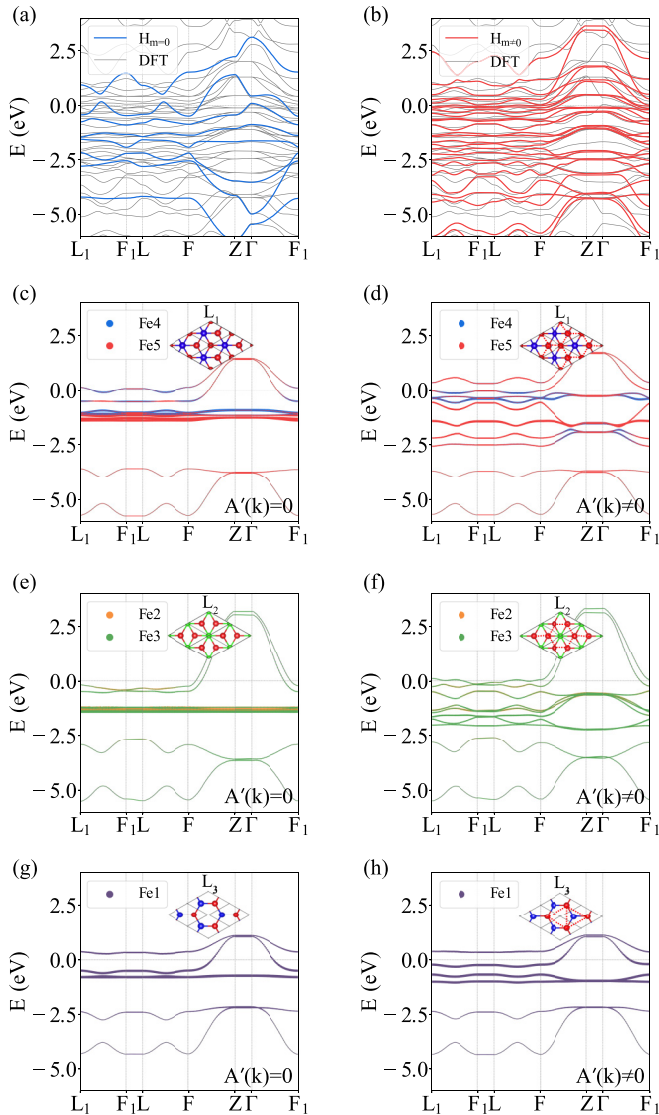


FIG. 3. Band structures by model Hamiltonians of  $\text{Fe}_5\text{GeTe}_2$ . (a, b) The band structures of  $H_{m=0}$  and  $H_{m\neq 0}$  in red and blue. The dashed gray lines are the band structures calculated by first-principles calculations. (c, d) Band structures by the  $H_{B_1}$  for  $A'(k) = 0$  (c) and  $A'(k) \neq 0$  (d). The projections of Fe4 and Fe5 are in blue and red, respectively. (e, f) Band structures by the  $H_{B_2}$  for  $A'(k) = 0$  (e) and  $A'(k) \neq 0$  (f). The projections of Fe4 and Fe5 are in orange and green, respectively. (g, h) Band structures by the  $H_{B_3}$  for  $A'(k) = 0$  (g) and  $A'(k) \neq 0$  (h). The projections of Fe1 are in purple.

properties of the BCL [57,58]. When  $N_A > N_B$ , the hopping along different directions overlaps destructively at the  $B$  sublattice, resulting in  $(N_A - N_B)$  states solely on the  $A$  sublattice at every momentum  $k$ . Since there are no hoppings between states on the  $A$  sublattice of BCL, these states form  $(N_A - N_B)$  flat bands. However, according to the proof in Appendix A, the crystal field splitting of orbitals due to the crystal field effect and the intrasublattice hoppings on  $A$  sublattice may lead to slight bending or loss of degeneracy in the flat bands. We will take into account the impact of the crystal field splitting and  $A'(k)$  on the flat bands when performing calculations using these model Hamiltonians.

We first analyze the flat bands according to the BCL Hamiltonian  $H_{B_i}$  of  $\text{Fe}_{n=4,5}\text{GeTe}_2$ . We first neglect the crystal field splitting of the  $d$  orbital due to the crystal field effect and the intrasublattice hoppings  $A'(k)$  for each BCL. The  $L_1/L_3$  BCL of  $\text{Fe}_4\text{GeTe}_2$  and  $L_3$  BCL of  $\text{Fe}_5\text{GeTe}_2$  are honeycomb lattices that consist of a Fe sublattice (denoted as the  $A$  sublattice) and a Te sublattice (denoted as the  $B$  sublattice). The  $A$  sublattice comprises four degenerate  $d$  orbitals, while the  $B$  sublattice comprises two degenerate  $p$  orbitals. As a result, the BCL Hamiltonian with  $(N_A - N_B = 2)$  degenerate flat bands. On the other hand, the  $L_2$  BCL of  $\text{Fe}_4\text{GeTe}_2$  and  $L_1/L_2$  BCLs of  $\text{Fe}_5\text{GeTe}_2$  are dice lattices that consist of the sublattice with two Fe (denoted as the  $A$  sublattice) and a Te/Ge sublattice (denoted as the  $B$  sublattice). The  $A$  sublattice contains eight degenerate  $d$  orbitals, while the  $B$  sublattice contains two degenerate  $p$  orbitals. The BCL Hamiltonian for this dice lattice has  $(N_A - N_B = 6)$  degenerate flat bands. Due to the relatively localized nature of the  $d$  orbitals, we anticipate that the intrasublattice hopping ( $A'(k)$ ) will have small magnitudes, thereby having a limited impact on the formation of flat bands.

Based on the model Hamiltonians, the flat bands are calculated, shown in Figs. 2(c), 2(e), 3(c), 3(e) and 3(g) without considering the intrasublattice hoppings in  $A$  sublattice ( $A'(k) = 0$ ) and Figs. 2(d), 2(f), 3(d), 3(f) and 3(h) with considering the intrasublattice hoppings ( $A'(k) \neq 0$ ). The clear flat bands have been shown in Figs. 2 and 3, though the  $A'(k) \neq 0$  lead to the slight bending of the nearly flat bands. We can see that the dispersion of the bands almost keep unchanged with  $A'(k) = 0$  and  $A'(k) \neq 0$  for  $L_1/L_3$  BCLs of  $\text{Fe}_4\text{GeTe}_2$  and  $L_3$  BCL of  $\text{Fe}_5\text{GeTe}_2$ , whereas this is not the case for the  $L_2$  BCL of  $\text{Fe}_4\text{GeTe}_2$  and  $L_1/L_2$  BCLs of  $\text{Fe}_5\text{GeTe}_2$  [Figs. 2(e), 2(f), 3(c)–3(f)] due to the hopping between orbitals of Fe in dice lattice. We find that the bands from BCL model Hamiltonians with  $A'(k) \neq 0$  can well reproduce the bands obtained from first-principles calculations, which support that the flat bands originate from the BCLs of  $\text{Fe}_{n=4,5}\text{GeTe}_2$ .

It is worth discussing whether the flat bands of  $\text{Fe}_{n=4,5}\text{GeTe}_2$  are itinerant or local. Flat bands can be classified into two types: trivial flat atomic bands and nontrivial flat bands [57]. Flat atomic bands originate from the localization of orbitals or isolated atoms, resulting in negligible overlaps between atomic wave functions [57]. Conversely, nontrivial flat bands emerge from extended wave functions with substantial overlaps and hoppings [57], indicating the itinerant character. In the case of  $\text{Fe}_{n=4,5}\text{GeTe}_2$ , the significant overlaps and hoppings between the orbitals suggest that their flat bands are itinerant.

### C. Flat-band ferromagnetism

In the absence of spin polarization, all flat bands formed by the  $d$  orbitals of Fe are close to the Fermi energy due to the partial occupation of the  $d$  orbitals. These flat bands result in sharp peaks of the non-spin-polarized density of states (DOS) near the Fermi energy. According to the Stoner theory, these peaks can lead to spontaneous magnetization [43,59,60]. The critical condition for the instability is expressed as  $U > 1/N_{E_F}$  [59], and here  $N_{E_F}$  denotes the DOS at the Fermi energy.

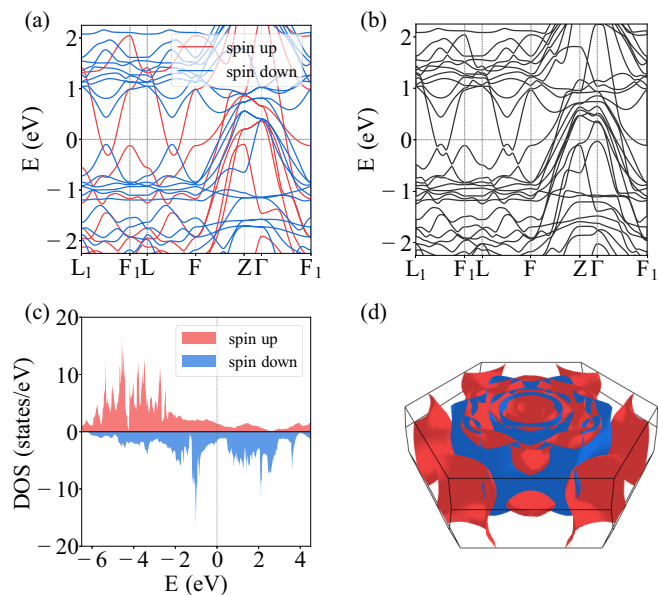


FIG. 4. Electronic structures of  $\text{Fe}_4\text{GeTe}_2$  calculated by first-principles calculations with  $U = 3.0$  eV. (a) The non-SOC band structure. (b) The SOC band structure. (c) The spin-polarized DOS without SOC. (d) The Fermi surfaces with up spin are in red, while the Fermi surfaces with down spin are in blue.

As the value of  $U$  increases, the energies of states with up and down spin will decrease and increase respectively, leading to a spin-polarized DOS. Consequently, flat bands near the Fermi energy in non-spin-polarized band structures can give rise to ferromagnetism. The spin-polarized DOS contributes to the magnetic moment, which can be quantified as  $m = n_\uparrow - n_\downarrow$ , where  $n_\uparrow/n_\downarrow$  represents the number of occupied states with the up/down spin. The magnetic moment increases with increasing  $U$ , which is also confirmed by the results of first-principles calculations [Figs. 5(a) and 7(a)].

## V. ELECTRONIC STRUCTURE AND MAGNETIC PROPERTIES

### A. $\text{Fe}_4\text{GeTe}_2$

We perform first-principles calculations to investigate the electronic structure and magnetic properties of  $\text{Fe}_4\text{GeTe}_2$ . In our calculations, we employ  $U = 3.0$  eV to obtain the band

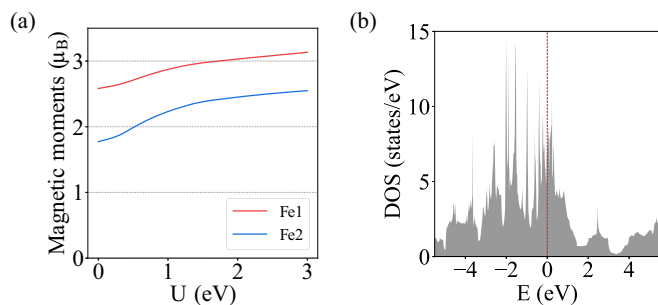


FIG. 5. Magnetic properties of  $\text{Fe}_4\text{GeTe}_2$  calculated by first-principles calculations. (a) The  $U$  dependence of magnetic moments of unequivalent Fe atoms. (b) The non-spin-polarized DOS.

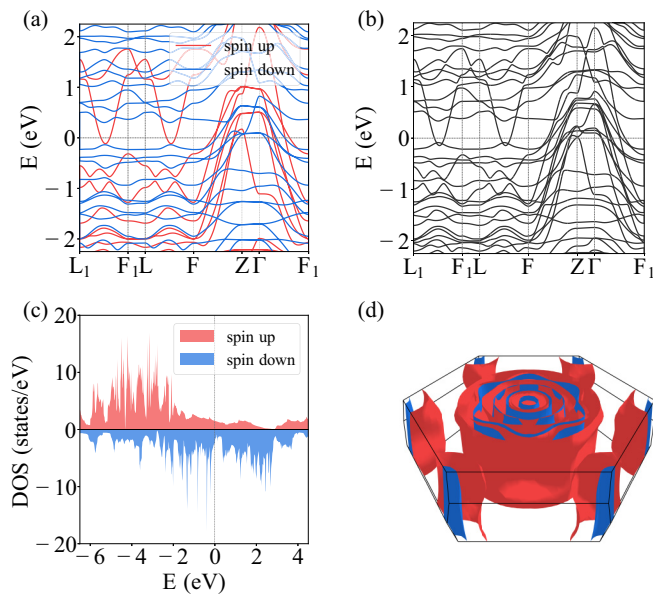


FIG. 6. Electronic structures of  $\text{Fe}_5\text{GeTe}_2$  calculated by first-principles calculations with  $U = 3.0$  eV. (a) The band structure without SOC. (b) The band structure with SOC. (c) The spin-polarized DOS without SOC. (d) The Fermi surfaces with up spin are in red, while the Fermi surfaces with down spin are in blue.

structure, DOS, and Fermi surfaces. The results suggest that the band structures with and without SOC are similar, implying that SOC has a negligible effect on the electronic structure of  $\text{Fe}_4\text{GeTe}_2$  [Figs. 4(a) and 4(b)]. The non-spin-polarized DOS indicates the  $N_{E_F}$  value is about 8.8 states/eV. Considering the Stoner criterion as  $U > 1/N_{E_F}$ ,  $\text{Fe}_4\text{GeTe}_2$  satisfying the Stoner criterion requires  $U$  to be greater than 0.11 eV. Although the precise value of  $U$  cannot be ascertained, according to this paper [11], the effective  $U$  value in  $\text{Fe}_4\text{GeTe}_2$  is significantly higher than 0.11 eV. Hence, our calculations indicate that  $\text{Fe}_4\text{GeTe}_2$  should meet the Stoner criterion. The spin-polarization DOS is consistent with the ferromagnetism [Fig. 4(c)]. The band structure and Fermi surfaces [Fig. 4(d)] indicate the  $\text{Fe}_4\text{GeTe}_2$  is a quasi-2D ferromagnetic metal.

By gradually increasing the  $U$ , we observe a gradual increase in the magnetic moments of the Fe atoms of  $\text{Fe}_4\text{GeTe}_2$ . As illustrated in Fig. 5(a), the magnetic moments of Fe1 (Fe1') and Fe2 (Fe2') surpass  $1.5 \mu_B$  when  $U = 0.0$  eV. Fur-

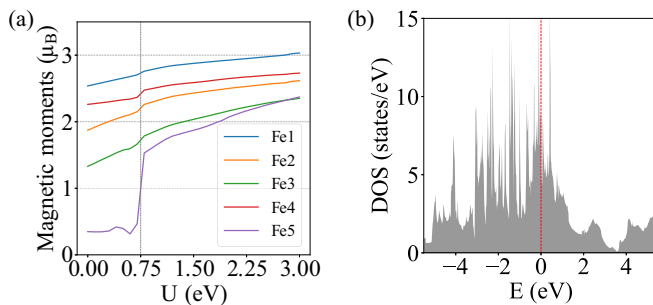


FIG. 7. Magnetic properties of  $\text{Fe}_5\text{GeTe}_2$  calculated by first-principles calculations. (a) The  $U$  dependence of magnetic moments of unequivalent Fe atoms. (b) The non-spin-polarized DOS.

thermore, we identify the presence of nearly flat bands in the non-spin-polarized band structures (Fig. 2) and the corresponding peaks in DOS [Fig. 5(b)]. These sharp peaks near the Fermi energy suggest that  $\text{Fe}_4\text{GeTe}_2$  exhibits characteristics of an itinerant flat-band ferromagnet [59].

### B. $\text{Fe}_5\text{GeTe}_2$

We further perform first-principles calculations to analyze the electronic and magnetic properties of  $\text{Fe}_5\text{GeTe}_2$ . As shown in Figs. 6 and 7, the band structures, DOS, and Fermi surfaces are similar to those of  $\text{Fe}_4\text{GeTe}_2$ . The non-spin-polarized DOS indicates the  $N_{E_F}$  value is about 7.4 states/eV. The effective value of  $U$  is greater than 0.14 eV [11], which satisfies the Stoner criterion. Therefore  $\text{Fe}_5\text{GeTe}_2$  should also be an itinerant ferromagnet.

However, there is a significant difference in the magnetic properties of Fe5. For  $U \leq 0.7$  eV, the magnetic moments of Fe5 are negligible, while it has a sudden increase between  $U = 0.7$  and 0.8 eV. We explain this phenomenon based on the band structure of the  $L_1$  BCL which is a quasi-dice lattice. The energy levels of Fe5 orbitals are slightly lower than those of Fe4 due to their different coupling to Te1. Then, bonding and anti-bonding bands are formed through the hopping between Fe4 and Fe5 orbitals. The anti-bonding band is primarily composed of Fe4 orbitals, whereas the bonding band is dominated by Fe5 orbitals. The Fe4-dominated bands are very close to the Fermi energy, resulting in the spontaneous magnetization of Fe4. As the value of  $U$  increases, the Fe5-dominated flat bands cross the Fermi level, leading to a pronounced enhancement in Fe5's magnetic moment.

We also investigate the effect of external pressure on the magnetic moment of Fe5 for  $\text{Fe}_5\text{GeTe}_2$ . For simplicity, the cell volume is kept unchanged, applying pressure along the  $z$  direction causes stretching in the  $xy$  plane. The compression along the  $z$  direction is primarily accommodated by the vdW gaps, resulting in negligible alteration to the vertical spacing among atoms within each octuple layer. Consequently, the pressure primarily influences the intralayer hoppings due to the in-plane stretching. Therefore the hopping between Fe4 and Fe5 slightly decreases, causing the energy level of Fe5 to approach the Fermi energy. Therefore the magnetic moment of Fe5 increases with the pressure in the  $z$  direction, as illustrated in Fig. 8. Though pressure-induced magnetic transitions of Fe5 may be detectable through neutron scattering [61], such measurements are relatively challenging. Our calculations find that the total magnetic moment changes with the magnetic variation of Fe5, which can be readily quantified. Therefore measuring the total magnetic moment is a more convenient approach to indicate the magnetic transitions of Fe5.

## VI. CONCLUSION

In this study, we investigate the origin of the nearly flat bands and ferrimagnetism in  $\text{Fe}_{n=4,5}\text{GeTe}_2$ . Our analysis reveals that the lattice structure of these materials can be viewed as three stacked BCLs along the  $z$  direction. The presence of different orbital numbers on two sublattices results in nearly flat bands. We demonstrate that the observed ferromagnetism

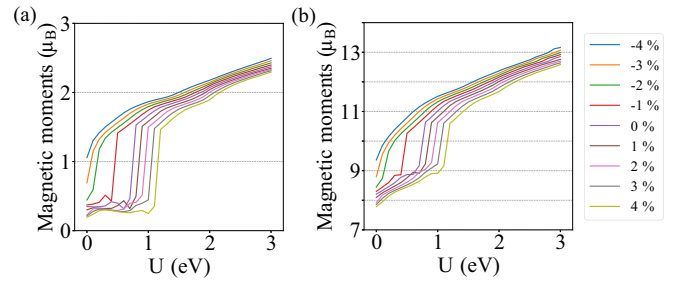


FIG. 8. The dependence of the magnetism of  $\text{Fe}_5\text{GeTe}_2$  on external pressures calculated by first-principles calculations. The percentages indicate the proportion of deformation in the  $z$ -direction. (a) The  $U$  dependence of Fe5's magnetic moments under different external pressures. (b) The  $U$  dependence of total magnetic moments under different external pressures.

in  $\text{Fe}_{n=4,5}\text{GeTe}_2$  arises from these nearly flat bands according to the Stoner theory. By combining model calculations with first-principles calculations, we find that the magnetic moment of Fe5 in  $\text{Fe}_5\text{GeTe}_2$  is sensitive to Coulomb interactions  $U$  and external pressure, which might be experimentally observed.

The emergence of flat-band ferromagnetism in  $\text{Fe}_{n=4,5}\text{GeTe}_2$  predominantly depends on the lattice structure, orbital characteristics, and electron filling number. These findings contribute to our understanding of the electronic and magnetic properties of vdW ferromagnets, specifically  $\text{Fe}_{n=4,5}\text{GeTe}_2$ .

## ACKNOWLEDGMENTS

This work is supported by National Key Projects for Research and Development of China (Grant No. 2021YFA1400400), the Fundamental Research Funds for the Central Universities (Grant No. 020414380185), Natural Science Foundation of Jiangsu Province (Grant No. BK20200007), the Natural Science Foundation of China (Grants No. 12074181, No. 12104217, and No. 11834006) and the Fok Ying-Tong Education Foundation of China (Grant No. 161006). Thanks to e-Science Center of Collaborative Innovation Center of Advanced Microstructures.

## APPENDIX: A BRIEF PROOF OF FLAT BANDS IN BCLs

Firstly we ignore the intrasublattice hoppings and the crystal field splitting of orbitals on the  $A$  sublattice, so  $A_k = \epsilon I$ , where  $I$  is an identity matrix and  $\epsilon$  is the onsite energies of orbitals on  $A$  sublattice. We set  $\epsilon$  as the zero energy point:

$$H_k = \begin{pmatrix} O & S_k \\ S_k^\dagger & B_k \end{pmatrix} \quad (\text{A1})$$

Diagonalizing  $N_B \times N_A$  rectangular matrix  $S_k$ , we have

$$S_k = W_k \Sigma_k V_k^\dagger \quad (\text{A2})$$



Here,  $\Sigma_k$  is a rectangular diagonal matrix with  $N_A - N_B$  zero rows:

$$\Sigma_k = \begin{pmatrix} \epsilon_1 & 0 & 0 & \dots & 0 \\ 0 & \epsilon_2 & 0 & \dots & 0 \\ 0 & 0 & \epsilon_3 & \ddots & 0 \\ \vdots & \ddots & \ddots & \ddots & 0 \\ 0 & 0 & \dots & 0 & \epsilon_{N_B} \\ 0 & 0 & \dots & 0 & 0 \\ \vdots & \vdots & \dots & \vdots & \vdots \\ 0 & 0 & \dots & 0 & 0 \end{pmatrix}. \quad (\text{A3})$$

Then we perform a similarity transformation on  $H_k$  as

$$H_k = \begin{pmatrix} W_k & O \\ O & V_k \end{pmatrix} \begin{pmatrix} O & \Sigma_k \\ \Sigma_k^\dagger & b_k \end{pmatrix} \begin{pmatrix} W_k^\dagger & O \\ O & V_k^\dagger \end{pmatrix}, \quad (\text{A4})$$

where  $b_k = V_k^{-1} B_k (V_k^\dagger)^{-1}$ . So that  $H_k$  is similar to a matrix that contains  $N_A - N_B$  zero rows, which implies that  $H_k$  possesses at least  $N_A - N_B$  zero-energy solutions with any  $k$ . Then we could conclude that a BCL has at least  $N_A - N_B$  degenerate flat bands at the onsite energy of orbitals on  $A$  sublattice. This proof does not make requirements on the form of  $B_k$ . Therefore intrasublattice hoppings and crystal field splitting of orbitals on the  $B$  sublattice do not affect the flat band.

- [1] S. Bera, S. K. Pradhan, M. S. Khan, R. Pal, B. Pal, S. Kalimuddin, A. Bera, B. Das, A. N. Pal, and M. Mondal, Unravelling the nature of spin reorientation transition in quasi-2d vdW magnetic material, Fe<sub>4</sub>GeTe<sub>2</sub>, *J. Magn. Magn. Mater.* **565**, 170257 (2023).
- [2] H. Chen, S. Asif, M. Whalen, J. Támara-Isaza, B. Luetke, Y. Wang, X. Wang, M. Ayako, S. Lamsal, A. F. May, M. A. McGuire, C. Chakraborty, J. Q. Xiao, and M. J. H. Ku, Revealing room temperature ferromagnetism in exfoliated Fe<sub>5</sub>GeTe<sub>2</sub> flakes with quantum magnetic imaging, *2D Mater.* **9**, 025017 (2022).
- [3] H. Chen, S. Asif, K. Dolui, Y. Wang, J. Támara-Isaza, V. M. L. D. P. Goli, M. Whalen, X. Wang, Z. Chen, H. Zhang, K. Liu, D. Jariwala, M. B. Jungfleisch, C. Chakraborty, A. F. May, M. A. McGuire, B. K. Nikolic, J. Q. Xiao, and M. J. H. Ku, Above-room-temperature ferromagnetism in thin van der waals flakes of cobalt-substituted Fe<sub>5</sub>GeTe<sub>2</sub>, *ACS Appl. Mater. Interfaces* **15**, 3287 (2023).
- [4] J. Seo, D. Y. Kim, E. S. An, K. Kim, G. Y. Kim, S. Y. Hwang, D. W. Kim, B. G. Jang, H. Kim, G. Eom, S. Y. Seo, R. Stania, M. Muntwiler, J. Lee, K. Watanabe, T. Taniguchi, Y. J. Jo, J. Lee, B. I. Min, M. H. Jo *et al.*, Nearly room temperature ferromagnetism in a magnetic metal-rich van der waals metal, *Sci. Adv.* **6**, eaay8912 (2020).
- [5] J. Stahl, E. Shlaen, and D. Johrendt, The van der waals ferromagnets Fe<sub>5- $\delta$</sub> GeTe<sub>2</sub> and Fe<sub>5- $\delta$ - $x$</sub> Ni <sub>$x$</sub> GeTe<sub>2</sub> crystal structure, stacking faults, and magnetic properties, *Zeitschrift für anorganische und allgemeine Chemie* **644**, 1923 (2018).
- [6] H. Wang, H. Lu, Z. Guo, A. Li, P. Wu, J. Li, W. Xie, Z. Sun, P. Li, H. Damas, A. M. Friedel, S. Migot, J. Ghanbaja, L. Moreau, Y. Fagot-Revurat, S. Petit-Watelot, T. Hauet, J. Robertson, S. Mangin, W. Zhao *et al.*, Interfacial engineering of ferromagnetism in wafer-scale van der waals Fe<sub>4</sub>GeTe<sub>2</sub> far above room temperature, *Nat. Commun.* **14**, 2483 (2023).
- [7] M. Tang, J. Huang, F. Qin, K. Zhai, T. Ideue, Z. Li, F. Meng, A. Nie, L. Wu, X. Bi, C. Zhang, L. Zhou, P. Chen, C. Qiu, P. Tang, H. Zhang, X. Wan, L. Wang, Z. Liu, Y. Tian *et al.*, Continuous manipulation of magnetic anisotropy in a van der waals ferromagnet via electrical gating, *Nat. Electron.* **6**, 28 (2023).
- [8] J. Seo, E. S. An, T. Park, S.-Y. Hwang, G.-Y. Kim, K. Song, W.-s. Noh, J. Y. Kim, G. S. Choi, M. Choi, E. Oh, K. Watanabe, T. Taniguchi, J. H. Park, Y. J. Jo, H. W. Yeom, S.-Y. Choi, J. H. Shim, and J. S. Kim, Tunable high-temperature itinerant antiferromagnetism in a van der waals magnet, *Nat. Commun.* **12**, 2844 (2021).
- [9] A. F. May, C. A. Bridges, and M. A. McGuire, Physical properties and thermal stability of Fe<sub>5- $x$</sub> GeTe<sub>2</sub> single crystals, *Phys. Rev. Mater.* **3**, 104401 (2019).
- [10] X. Chen, Y.-T. Shao, R. Chen, S. Susarla, T. Hogan, Y. He, H. Zhang, S. Wang, J. Yao, P. Ercius, D. A. Muller, R. Ramesh, and R. J. Birgeneau, Pervasive beyond room-temperature ferromagnetism in a doped van der waals magnet, *Phys. Rev. Lett.* **128**, 217203 (2022).
- [11] S. Ghosh, S. Ershadrad, V. Borisov, and B. Sanyal, Unraveling effects of electron correlation in two-dimensional Fe <sub>$n$</sub> GeTe<sub>2</sub> ( $n = 3, 4, 5$ ) by dynamical mean field theory, *npj Comput. Mater.* **9**, 86 (2023).
- [12] S. Mondal, N. Khan, S. M. Mishra, B. Satpati, and P. Mandal, Critical behavior in the van der waals itinerant ferromagnet Fe<sub>4</sub>GeTe<sub>2</sub>, *Phys. Rev. B* **104**, 094405 (2021).
- [13] A. F. May, D. Ovchinnikov, Q. Zheng, R. Hermann, S. Calder, B. Huang, Z. Fei, Y. Liu, X. Xu, and M. A. McGuire, Ferromagnetism near room temperature in the cleavable van der waals crystal Fe<sub>5</sub>GeTe<sub>2</sub>, *ACS Nano* **13**, 4436 (2019).
- [14] L. Alahmed, B. Nepal, J. Macy, W. Zheng, B. Casas, A. Sapkota, N. Jones, A. R. Mazza, M. Brahlek, W. Jin, M. Mahjouri-Samani, S. S. L. Zhang, C. Mewes, L. Balicas, T. Mewes, and P. Li, Magnetism and spin dynamics in room-temperature van der waals magnet Fe<sub>5</sub>GeTe<sub>2</sub>, *2D Mater.* **8**, 045030 (2021).
- [15] H. Zhang, R. Chen, K. Zhai, X. Chen, L. Caretta, X. Huang, R. V. Chopdekar, J. Cao, J. Sun, J. Yao, R. Birgeneau, and R. Ramesh, Itinerant ferromagnetism in van der waals Fe<sub>5- $x$</sub> GeTe<sub>2</sub> crystals above room temperature, *Phys. Rev. B* **102**, 064417 (2020).
- [16] Q. Liu, J. Xing, Z. Jiang, Y. Guo, X. Jiang, Y. Qi, and J. Zhao, Layer-dependent magnetic phase diagram in Fe <sub>$n$</sub> GeTe<sub>2</sub> ( $3 \leq n \leq 7$ ) ultrathin films, *Commun. Phys.* **5**, 140 (2022).
- [17] C. Tan, W.-Q. Xie, G. Zheng, N. Aloufi, S. Albarakati, M. Algarni, J. Li, J. Partridge, D. Culcer, X. Wang, J. B. Yi, M. Tian, Y. Xiong, Y.-J. Zhao, and L. Wang, Gate-controlled magnetic phase transition in a van der waals magnet Fe<sub>5</sub>GeTe<sub>2</sub>, *Nano Lett.* **21**, 5599 (2021).

- [18] C. Gong and X. Zhang, Two-dimensional magnetic crystals and emergent heterostructure devices, *Science* **363**, eaav4450 (2019).
- [19] K. S. Burch, D. Mandrus, and J. Park, Magnetism in two-dimensional van der waals materials, *Nature (London)* **563**, 47 (2018).
- [20] C. Gong, L. Li, Z. Li, H. Ji, A. Stern, Y. Xia, T. Cao, W. Bao, C. Wang, Y. Wang, Z. Q. Qiu, R. J. Cava, S. G. Louie, J. Xia, and X. Zhang, Discovery of intrinsic ferromagnetism in two-dimensional van der waals crystals, *Nature (London)* **546**, 265 (2017).
- [21] B. Huang, G. Clark, E. Navarro-Moratalla, D. R. Klein, R. Cheng, K. L. Seyler, D. Zhong, E. Schmidgall, M. A. McGuire, D. H. Cobden, W. Yao, D. Xiao, P. Jarillo-Herrero, and X. Xu, Layer-dependent ferromagnetism in a van der waals crystal down to the monolayer limit, *Nature (London)* **546**, 270 (2017).
- [22] Y. Deng, Y. Yu, Y. Song, J. Zhang, N. Z. Wang, Z. Sun, Y. Yi, Y. Z. Wu, S. Wu, J. Zhu, J. Wang, X. H. Chen, and Y. Zhang, Gate-tunable room-temperature ferromagnetism in two-dimensional  $\text{Fe}_3\text{GeTe}_2$ , *Nature (London)* **563**, 94 (2018).
- [23] Z. Fei, B. Huang, P. Malinowski, W. Wang, T. Song, J. Sanchez, W. Yao, D. Xiao, X. Zhu, A. F. May, W. Wu, D. H. Cobden, J.-H. Chu, and X. Xu, Two-dimensional itinerant ferromagnetism in atomically thin  $\text{Fe}_3\text{GeTe}_2$ , *Nat. Mater.* **17**, 778 (2018).
- [24] D. Li, S. Haldar, T. Drevelow, and S. Heinze, Tuning the magnetic interactions in van der waals  $\text{Fe}_3\text{GeTe}_2$  heterostructures: A comparative study of *ab initio* methods, *Phys. Rev. B* **107**, 104428 (2023).
- [25] H. L. Zhuang, P. R. C. Kent, and R. G. Hennig, Strong anisotropy and magnetostriction in the two-dimensional stoner ferromagnet  $\text{Fe}_3\text{GeTe}_2$ , *Phys. Rev. B* **93**, 134407 (2016).
- [26] L. Zhou, J. Huang, M. Tang, C. Qiu, F. Qin, C. Zhang, Z. Li, D. Wu, and H. Yuan, Gate-tunable spin valve effect in  $\text{Fe}_3\text{GeTe}_2$ -based van der waals heterostructures, *InfoMat* **5**, e12371 (2023).
- [27] Y. Huang, X. Yao, F. Qi, W. Shen, and G. Cao, Anomalous resistivity upturn in the van der waals ferromagnet  $\text{Fe}_5\text{GeTe}_2$ , *Appl. Phys. Lett.* **121**, 162403 (2022).
- [28] Y. Deng, Z. Xiang, B. Lei, K. Zhu, H. Mu, W. Zhuo, X. Hua, M. Wang, Z. Wang, G. Wang, M. Tian, and X. Chen, Layer-number-dependent magnetism and anomalous hall effect in van der waals ferromagnet  $\text{Fe}_5\text{GeTe}_2$ , *Nano Lett.* **22**, 9839 (2022).
- [29] X. Yang, X. Zhou, W. Feng, and Y. Yao, Strong magneto-optical effect and anomalous transport in the two-dimensional van der waals magnets  $\text{Fe}_n\text{GeTe}_2$  ( $n = 3, 4, 5$ ), *Phys. Rev. B* **104**, 104427 (2021).
- [30] T. Ohta, M. Tokuda, S. Iwakiri, K. Sakai, B. Driesen, Y. Okada, K. Kobayashi, and Y. Niimi, Butterfly-shaped magnetoresistance in van der waals ferromagnet  $\text{Fe}_5\text{GeTe}_2$ , *AIP Adv.* **11**, 025014 (2021).
- [31] X. Lv, K. Pei, C. Yang, G. Qin, M. Liu, J. Zhang, and R. Che, Controllable topological magnetic transformations in the thickness-tunable van der waals ferromagnet  $\text{Fe}_5\text{GeTe}_2$ , *ACS Nano* **16**, 19319 (2022).
- [32] C. Zhang, C. Liu, S. Zhang, B. Zhou, C. Guan, Y. Ma, H. Algaidi, D. Zheng, Y. Li, X. He, J. Zhang, P. Li, Z. Hou, G. Yin, K. Liu, Y. Peng, and X.-X. Zhang, Magnetic skyrmions with unconventional helicity polarization in a van der waals ferromagnet, *Adv. Mater.* **34**, 2204163 (2022).
- [33] M. Schmitt, T. Denneulin, A. Kovács, T. G. Saunderson, P. Rübmann, A. Shahee, T. Scholz, A. H. Tavabi, M. Gradhand, P. Mavropoulos, B. V. Lotsch, R. E. Dunin-Borkowski, Y. Mokrousov, S. Blügel, and M. Kläui, Skyrmionic spin structures in layered  $\text{Fe}_5\text{GeTe}_2$  up to room temperature, *Commun. Phys.* **5**, 254 (2022).
- [34] B. Sutherland, Localization of electronic wave functions due to local topology, *Phys. Rev. B* **34**, 5208 (1986).
- [35] D. Călugăru, A. Chew, L. Elcoro, Y. Xu, N. Regnault, Z.-D. Song, and B. A. Bernevig, General construction and topological classification of crystalline flat bands, *Nat. Phys.* **18**, 185 (2022).
- [36] B. Wu, S. Fang, J. Yang, S. Liu, Y. Peng, Q. Li, Z. Lin, J. Shi, W. Yang, Z. Luo, C. Wang, J. Yang, J. Lu, and H. Du, High-performance  $\text{Fe}_x\text{GeTe}_2$ -based ( $x = 4$  or  $5$ ) van der waals magnetic tunnel junctions, *Phys. Rev. Appl.* **19**, 024037 (2023).
- [37] D. Kim, C. Lee, B. G. Jang, K. Kim, and J. H. Shim, Drastic change of magnetic anisotropy in  $\text{Fe}_3\text{GeTe}_2$  and  $\text{Fe}_4\text{GeTe}_2$  monolayers under electric field studied by density functional theory, *Sci. Rep.* **11**, 17567 (2021).
- [38] M. Joe, U. Yang, and C. Lee, First-principles study of ferromagnetic metal  $\text{Fe}_5\text{GeTe}_2$ , *Nano Materials Science* **1**, 299 (2019).
- [39] K. Yamagami, Y. Fujisawa, B. Driesen, C. H. Hsu, K. Kawaguchi, H. Tanaka, T. Kondo, Y. Zhang, H. Wadati, K. Araki, T. Takeda, Y. Takeda, T. Muro, F. C. Chuang, Y. Niimi, K. Kuroda, M. Kobayashi, and Y. Okada, Itinerant ferromagnetism mediated by giant spin polarization of the metallic ligand band in the van der waals magnet  $\text{Fe}_5\text{GeTe}_2$ , *Phys. Rev. B* **103**, L060403 (2021).
- [40] E. H. Lieb, Two theorems on the Hubbard model, *Phys. Rev. Lett.* **62**, 1201 (1989).
- [41] O. Derzhko, J. Richter, and M. Maksymenko, Strongly correlated flat-band systems: The route from heisenberg spins to hubbard electrons, *Int. J. Mod. Phys. B* **29**, 1530007 (2015).
- [42] A. Mielke, Ferromagnetism in the hubbard model on line graphs and further considerations, *J. Phys. A: Math. Gen.* **24**, 3311 (1991).
- [43] A. Mielke, Ferromagnetism in the Hubbard model and hund's rule, *Phys. Lett. A* **174**, 443 (1993).
- [44] H. Tasaki, From nagaoka's ferromagnetism to flat-band ferromagnetism and beyond: An introduction to ferromagnetism in the hubbard model, *Prog. Theor. Phys.* **99**, 489 (1998).
- [45] H. Tasaki, Stability of ferromagnetism in hubbard models with nearly flat bands, *J. Stat. Phys.* **84**, 535 (1996).
- [46] K. Kusakabe and H. Aoki, Ferromagnetic spin-wave theory in the multiband hubbard model having a flat band, *Phys. Rev. Lett.* **72**, 144 (1994).
- [47] G. Kresse and D. Joubert, From ultrasoft pseudopotentials to the projector augmented-wave method, *Phys. Rev. B* **59**, 1758 (1999).
- [48] G. Kresse and J. Furthmüller, Efficient iterative schemes for *ab initio* total-energy calculations using a plane-wave basis set, *Phys. Rev. B* **54**, 11169 (1996).
- [49] G. Kresse and J. Furthmüller, Efficiency of *ab-initio* total energy calculations for metals and semiconductors using a plane-wave basis set, *Comput. Mater. Sci.* **6**, 15 (1996).
- [50] G. Kresse, J. Furthmüller, and J. Hafner, Theory of the crystal structures of selenium and tellurium: The effect of generalized-



- gradient corrections to the local-density approximation, *Phys. Rev. B* **50**, 13181 (1994).
- [51] G. Pizzi, V. Vitale, R. Arita, S. Blügel, F. Freimuth, G. Géranton, M. Gibertini, D. Gresch, C. Johnson, T. Koretsune, J. Ibañez-Azpiroz, H. Lee, J.-M. Lihm, D. Marchand, A. Marrazzo, Y. Mokrousov, J. I. Mustafa, Y. Nohara, Y. Nomura, L. Paulatto *et al.*, Wannier90 as a community code: New features and applications, *J. Phys.: Condens. Matter* **32**, 165902 (2020).
- [52] N. Marzari and D. Vanderbilt, Maximally localized generalized wannier functions for composite energy bands, *Phys. Rev. B* **56**, 12847 (1997).
- [53] I. Souza, N. Marzari, and D. Vanderbilt, Maximally localized wannier functions for entangled energy bands, *Phys. Rev. B* **65**, 035109 (2001).
- [54] D. Leykam, A. Andreanov, and S. Flach, Artificial flat band systems: from lattice models to experiments, *Adv. Phys.: X* **3**, 1473052 (2018).
- [55] P. O. Sukhachov, D. O. Oriekhov, and E. V. Gorbar, Stackings and effective models of bilayer dice lattices, *Phys. Rev. B* **108**, 075166 (2023).
- [56] P. O. Sukhachov, D. O. Oriekhov, and E. V. Gorbar, Optical conductivity of bilayer dice lattices, *Phys. Rev. B* **108**, 075167 (2023).
- [57] N. Regnault, Y. Xu, M.-R. Li, D.-S. Ma, M. Jovanovic, A. Yazdani, S. S. P. Parkin, C. Felser, L. M. Schoop, N. P. Ong, R. J. Cava, L. Elcoro, Z.-D. Song, and B. A. Bernevig, Catalogue of flat-band stoichiometric materials, *Nature (London)* **603**, 824 (2022).
- [58] Z. Li, J. Zhuang, L. Wang, H. Feng, Q. Gao, X. Xu, W. Hao, X. Wang, C. Zhang, K. Wu, S. X. Dou, L. Chen, Z. Hu, and Y. Du, Realization of flat band with possible nontrivial topology in electronic kagome lattice, *Sci. Adv.* **4**, eaau4511 (2018).
- [59] J. Kübler, *Theory of Itinerant Electron Magnetism, 2nd Edition* (Oxford University Press, 2021).
- [60] J. Wahle, N. Blümer, J. Schlipf, K. Held, and D. Vollhardt, Microscopic conditions favoring itinerant ferromagnetism, *Phys. Rev. B* **58**, 12749 (1998).
- [61] A. F. May, S. Calder, C. Cantoni, H. Cao, and M. A. McGuire, Magnetic structure and phase stability of the van der waals bonded ferromagnet  $\text{Fe}_{3-x}\text{GeTe}_2$ , *Phys. Rev. B* **93**, 014411 (2016).